Highly Viscous States Affect the Browning of Atmospheric Organic Particulate Matter

ACS central science

Research Article

Cite This: ACS Cent. Sci. 2018, 4, 207−215

Highly Viscous States Affect the Browning of Atmospheric Organic Particulate Matter

Pengfei Liu,[†] Yong Jie Li,[†,‡] Yan Wang,[†,§] Adam P. Bateman,[†] Yue Zhang,[†,∥] Zhaoheng Gong,[†] Allan K. Bertram,[⊥] and Scot T. Martin*[,†,#]

[†]John A. Paulson School of Engineering and Applied Sciences and [#]Department of Earth and Planetary Sciences, Harvard University, Cambridge, Massachusetts 02138, United States

[‡]Department of Civil and Environmental Engineering, Faculty of Science and Technology, University of Macau, Macau, China

[§]T. H. Chan School of Public Health, Harvard University, Boston, Massachusetts 02115, United States

[∥]Aerodyne Research Inc., Billerica, Massachusetts 01821, United States

[⊥]Department of Chemistry, University of British Columbia, Vancouver, British Columbia, Canada

Supporting Information

ABSTRACT: Initially transparent organic particulate matter (PM) can become shades of light-absorbing brown via atmospheric particle-phase chemical reactions. The production of nitrogen-containing compounds is one important pathway for browning. Semisolid or solid physical states of organic PM might, however, have sufficiently slow diffusion of reactant molecules to inhibit browning reactions. Herein, organic PM of secondary organic material (SOM) derived from toluene, a common SOM precursor in anthropogenically affected environments, was exposed to ammonia at different values of relative humidity (RH). The production of light-absorbing organonitrogen imines from ammonia exposure, detected by mass spectrometry and ultraviolet−visible spectrophotometry, was kinetically inhibited for RH < 20% for exposure times of 6 min to 24 h. By comparison, from 20% to 60% RH organonitrogen production took place, implying ammonia uptake and reaction. Correspondingly, the absorption index k across 280 to 320 nm increased from 0.012 to 0.02, indicative of PM browning. The k value across 380 to 420 nm increased from 0.001 to 0.004. The observed RH-dependent behavior of ammonia uptake and browning was well captured by a model that considered the diffusivities of both the large organic molecules that made up the PM and the small reactant molecules taken up from the gas phase into the PM. Within the model, large-molecule diffusivity was calculated based on observed SOM viscosity and evaporation. Small-molecule diffusivity was represented by the water diffusivity measured by a quartz-crystal microbalance. The model showed that the browning reaction rates at RH < 60% could be controlled by the low diffusivity of the large organic molecules from the interior region of the particle to the reactive surface region. The results of this study have implications for accurate modeling of atmospheric brown carbon production and associated influences on energy balance.

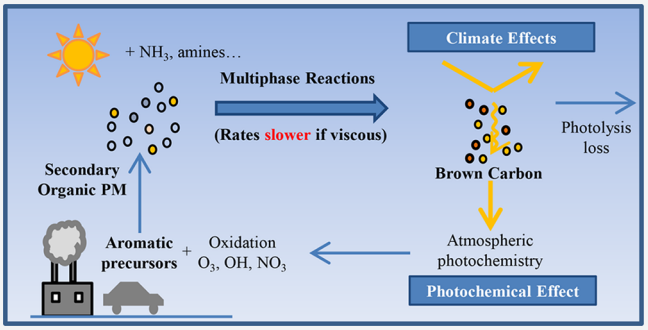

1. INTRODUCTION

Atmospheric particulate matter (PM) can directly and indirectly affect global climate[1] and adversely impact human health.[2,3] PM also participates in atmospheric chemical cycles through uptake, reaction, and release of trace gases.[4,5] Organic material comprises a large fraction of the submicron particulate mass suspended in the atmosphere.[6,7] Some organic PM absorbs light in the ultraviolet-to-visible region, and the absorption typically has a strong wavelength dependence.[8−10] This light-absorbing organic PM, commonly referred to as "brown carbon," can redistribute the absorption of radiation, at times leading to warming in the lower troposphere with attendant effects on climate radiative forcing and photochemistry.[11−13]

Brown carbon can be directly emitted from primary sources,[8,14] such as biomass burning,[15] or produced in the atmosphere as secondary organic material (SOM).[16−18] Light absorption by SOM depends on precursor type as well as the oxidation pathways active in its production. For example, SOM derived from aromatic precursors tends to be more than an order of magnitude more absorptive than that derived from terpenoid precursors.[17] The presence of molecular heteroatoms, such as nitrogen and sulfur, can further enhance light absorption.[19−21] The physicochemical properties of organic particles, including optical properties, dynamically evolve during the PM lifetime in the atmosphere.[7,22] The reactive

Received: September 27, 2017
Published: January 17, 2018

DOI: 10.1021/acscentsci.7b00452
ACS Cent. Sci. 2018, 4, 207−215

uptake of gaseous molecules and particle-phase chemistry can produce chromophores.[18,23] Uptake and particle-phase reactions of ammonia to produce imines can enhance light absorption for several types of SOM.[16] Chromophores can also be photobleached by photolysis and reactions with atmospheric oxidants.[22,24]

Although the detailed reactions governing the evolution of brown carbon are complex, an important governing factor might be the phase state of the SOM. Diffusivity in this reaction matrix might under some conditions be low enough to determine overall rates of chemical reaction,[25−27] both toward chromophore production and loss.[28,29] Until recently, organic PM was modeled as a low-viscosity liquid,[30] implying that the transformation and interactions between light-absorbing compounds and gas-phase species can occur throughout the particle volume for typically sized accumulation-mode atmospheric particles. The assumption of low viscosity, however, is challenged by recent observations.[31−33] Many organic compounds and their mixtures form amorphous solid or semisolid states upon dehydration.[34] Ambient and laboratory organic particles can rebound at moderate relative humidity (RH) upon impact with a hard surface, indicating that these particles are not liquid.[31,35,36] Depending on viscosity η, the physical state of the rebounding particles can be solid (i.e., glassy, $\eta > 10^{12}$ Pa s) or semisolid (i.e., η of 10^2 to 10^{12} Pa s). Direct viscosity measurements have been made for several types of SOM,[37−41] and the Stokes−Einstein relation linked the measured viscosities to inferred diffusivities for large organic molecules.[27] This relation, however, can break down for the diffusion of small molecules within a matrix of larger molecules[42,43] or in the vicinity of the glass transition.[44−46] Glass transition temperatures have been measured for several atmospherically relevant organic compounds,[47−49] and SOM is believed to become glassy at temperatures representative of the upper troposphere, with possible implications for ice nucleation processes.[50−55] The possibility that SOM might become glassy in the lower atmosphere at warmer temperatures and lower RH remains a topic of continuing research.[55−58]

High viscosities suggest that diffusivities can become sufficiently low to impose kinetic limitations on the rates of particle-phase reactions for time scales relevant to atmospheric processes. Even so, there can be significant differences between transitions in physical properties (i.e., rebound and liquefaction) and transitions in chemical reactivity or regimes of gas-particle partitioning. Li et al.,[25] for example, observed sharp increases in chemical reactivity at 20% RH for toluene-derived SOM aerosol particles. Liu et al.[56] likewise observed a nonlabile-to-labile transition at 20% RH for evaporation of semivolatile organic compounds (SVOCs) from toluene-derived SOM films. These transition RH values were significantly lower than the transition RH of 65% for particle rebound.[36] Accurate predictions of transitions in chemical reactivity should take into account the interplay among diffusivity, chemical rate constants, and particle size (cf. Figure 1a). In this regard, several kinetic models have included explicit treatment of reactant diffusivities.[59−63] The key parameters in these models were the diffusivity values of small molecules, such as OH, O_3, NO_3, H_2O, NH_3, and amines, as well as the diffusivity values of large organic molecules constituting the particle matrix.[27,61,62] The lack of data for constraining the values of these parameters, however, hindered model

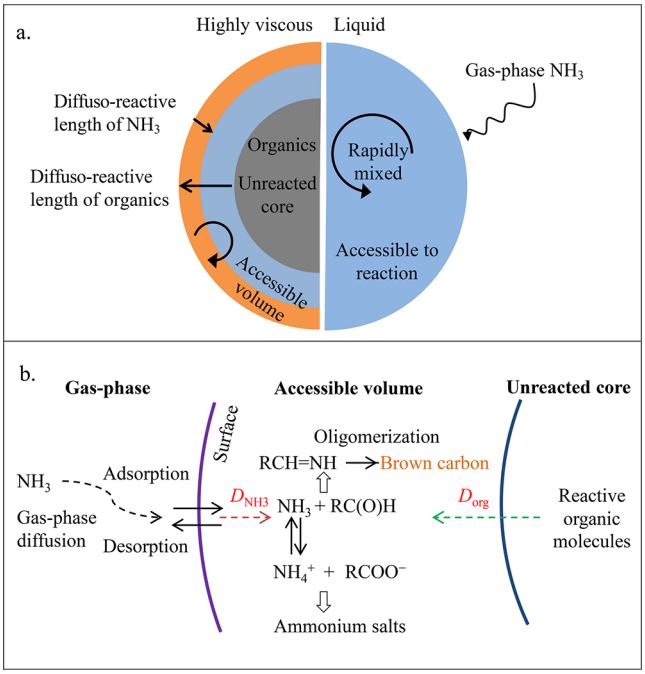

Figure 1. (a) Schematic of ammonia reactive uptake for a highly viscous droplet in the left panel and a well-mixed liquid droplet in the right panel. The accessible reactive volume is highlighted in both panels. (b) A simplified mechanism of ammonia uptake and brown carbon production for SOM derived from aromatic precursors. For instance, SOM carbonyls can react with ammonia to produce imines, which in turn oligomerize to yield conjugated light-absorbing organonitrogen compounds.[67] This browning pathway competes with other reactions that may not produce chromophores, such as the NH_3-neutralization of SOM carboxylic acids to form ammonium salts.[25,26,68]

confidence, including the modeling of secondary brown carbon production along in-particle chemical pathways.

As a focus of interpretation and analysis of the study described herein, the hypothesis is that slow diffusion associated with the high viscosity can limit rates of mass transfer and hence rates of condensed-phase reactions, including the reactions that produce brown carbon (cf. Figure 1a−b). The experiments described herein combined three types of measurements to investigate how highly viscous states can affect the browning of atmospheric organic particulate matter. (1) Particle-phase mass spectra were recorded following exposure of SOM particles to ammonia. The analysis focused on the production of organonitrogen imines (-C═N). Although these species only accounted for on the order of 10% of nitrogen uptake,[25] they can contribute to most of the light absorption (Figure 1b). The production of ammonium salts, which are typically not light absorbing, was presented in ref 25 for the same experiments. (2) Absorption spectra after ammonia exposure were recorded using an ultraviolet−visible spectrophotometer (UV−vis). The production of brown carbon was assessed from these data sets. (3) The water desorption rates from SOM thin films were measured using a quartz-crystal microbalance (QCM). Diffusivity values of small molecules were obtained through analysis of these data sets and used to estimate diffusion rates of ammonia within SOM.

The experiments focused on the reactions of ammonia with toluene-derived SOM. Toluene-derived SOM was chosen to represent a class of anthropogenic contributions to the

DOI: 10.1021/acscentsci.7b00452
ACS Cent. Sci. 2018, 4, 207−215

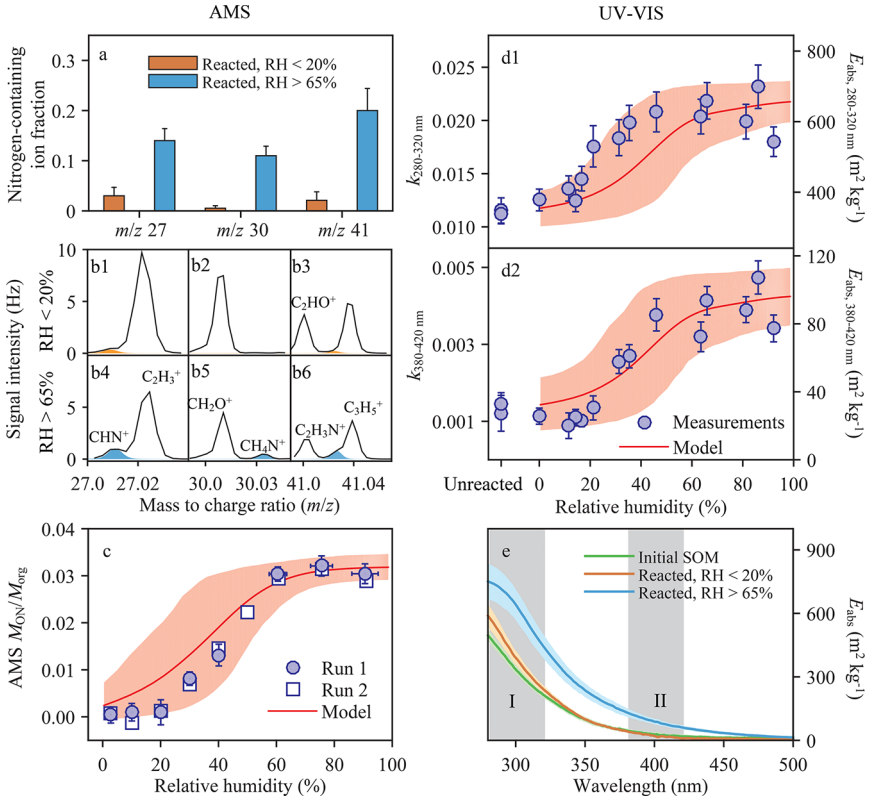

Figure 2. Organonitrogen production and changed optical properties of toluene-derived SOM exposed to ammonia at different RH values. (a) Nitrogen-containing ion fraction calculated as the signal intensity of each nitrogen-containing ion normalized by the signal intensity of the most abundant ion at the same nominal mass. Results are shown for toluene-derived SOM reacted with ammonia for high and low RH. (b1−b6) High-resolution mass spectral features corresponding to panel (a), showing isolation of the nitrogen-containing ion. (c) The ratio of organonitrogen mass concentration M_{ON} to total organic mass concentration M_{org} at different RH values. Error bars represent the estimated measurement uncertainty. Red shading represents the model error associated with the uncertainties of input parameters. (d1) Absorptive indices k on left axis and mass absorption coefficients E_{abs} on right axis from 280−320 nm for toluene-derived SOM. (d2) Same as panel (d1) but for 380−420 nm. The red curves in panels (c), (d1), and (d2) represent model results based on obtained diffusivities (i.e., Figure 3b,c). (e) Mass absorption coefficient as a function of wavelength for SOM-laden Teflon filters for initial conditions, ammonia-exposed conditions at low RH (<20% RH), and ammonia-exposed conditions at high RH (>65%). Shading regions I and II denote the spectral window represented in panels d1 and d2, respectively.

atmosphere.[64] Toluene-derived SOM produced under low-NO_x conditions is weakly light absorbing.[17] The absorption can be greatly enhanced, however, in the presence of nitrogen-containing compounds.[17,65,66] An important source of light-absorbing nitrogen-containing species can be the multiphase reactions between ammonia and SOM, as illustrated in Figure 1b.[16,21,23] Toluene-derived SOM has high viscosity at low RH. It becomes brittle for <20% RH.[40] The high viscosity can impose mass transfer limitations on rates of evaporation, uptake, and in-particle mixing of semivolatile compounds.[56,58] The limitations disappear at elevated RH because water can act as a plasticizer and soften the material.[48]

2. RESULTS AND DISCUSSION

2.1. Highly Viscous States and Brown Carbon Production. In a first set of experiments, a particle population of toluene-derived SOM was exposed to 5 ppm ammonia for a reactor residence time of 370 s in a continuous-flow mixing volume (cf. Supporting Information, Section S1 and Figure S1). After the reaction, the abundance of the nitrogen-containing ions produced for RH > 65% was 5−20 times higher than that produced for RH < 20% (Figure 2a). The produced organonitrogen imines were quantified by the $C_xH_yN_z^+$ ion family by the high-resolution mass spectrometry (Figure 2b) and used to determine the mass concentration M_{ON} of organonitrogen. The organonitrogen mass fraction, given by the ratio M_{ON}/M_{org} where M_{org} represents the mass concentration of total organic species, is plotted in Figure 2c for different values of relative humidity. The fraction increases from low to high RH. The interpretation is that diffusion limitations on mass transfer in highly viscous SOM completely inhibited the production of organonitrogen species for RH < 20% (Figure 2a).[40] A transition from diffusion-limited to saturated uptake occurred across 20% to 60% RH, which is consistent with previous viscosity measurements showing that this type of SOM is semisolid across this RH range.[36,40] Above 60% RH, the fraction M_{ON}/M_{org} did not change for further increases in RH, which is consistent with the behavior of liquid SOM in this RH range.[36,40] Diffusion was rapid in the liquid, meaning that it became quickly saturated with NH_3 and diffusion did not limit rates of reaction.

In a second set of experiments, optical properties were studied. Teflon filters laden with toluene-derived SOM were exposed to 500 ppb ammonia at fixed RH for 24 h (Supporting Information, Section S2). The RH among different experiments was varied from <5% to 90%. After ammonia exposure, browning of the filters was observed for RH > 65% but not for RH < 20%. Initial and reacted samples were extracted in methanol, and absorption spectra were recorded using an ultraviolet−visible spectrophotometer.

DOI: 10.1021/acscentsci.7b00452
ACS Cent. Sci. 2018, 4, 207−215

The absorptive indices k and the mass absorption coefficients E_{abs} were calculated, and the results are shown in Figure 2d,e (cf. Supporting Information, Section S2).[17] As a point of reference, a k value of 0.004 is typical of brown carbon in the urban atmosphere in a window of 380−420 nm.[69] The experiments herein found that k = 0.001 ± 0.0005 for the initial toluene SOM, meaning that the material was initially weakly absorbing. The value of k did not change significantly when exposed to ammonia for RH < 20%. It increased, however, to 0.004 ± 0.001 for toluene SOM exposed to ammonia at RH > 65%. Further results as a function of relative humidity are shown in Figure 2d1 for a band from 280 to 320 nm and in Figure 2d2 for a band from 380 to 420 nm. Solar radiation in the these two bands regulates the photolysis of O_3 and NO_2, respectively.[17]

The results show that the enhancement of light absorption strongly depended on RH (Figure 2d1 and 2d2). As the RH increased from less than 20% to greater than 60%, $k_{280-320}$ and $k_{380-420}$ increased by 50% and 400%, respectively. The dependence of chromophore-production on RH agreed with the RH dependence of organonitrogen production, although the two experiments had different exposure times and characteristic length scales (i.e., the radius of the particle or the thickness of the film) (cf. Table S1). These experimental results can be explained by the diffusion limitations on reaction rates.

A model was developed to capture the RH-dependent behavior of the production of organonitrogen species (Figure 2c) and the altered optical properties (Figure 2d1 and 2d2) (cf. Section S3). The complex chemical mechanisms were subsumed in the model as an effective second-order reaction between ammonia and the reactive organic species in the SOM matrix. Processes included (1) the uptake of NH_3 at the surface of the SOM under the assumption of rapid Henry's law equilibration between the gas phase and surface region (Figure 1b), (2) the diffusion of the small ammonia molecule into the SOM matrix (Figure 1a), (3) the diffusion of large reactive organic molecules from the interior region of the SOM to its surface (Figure 1a), and (4) chemical reactions and depletion of both reactants (Figure 1b). Both diffusivities in processes (2) and (3) depended on the water content of the SOM and hence on RH. At low RH, either or both diffusion processes limited rates of mass transfer and observed reaction rates.

Regimes of possible mass-transfer limitations on overall rates of reaction were considered within the model framework of accessible reaction volume.[61] This volume depended on the reacto-diffusion lengths of both ammonia and reactive organic species. The reacto-diffusion length, representing the characteristic distance that a typical reactant diffuses before reaction, depended on the reactant diffusivity and the reaction rate (Supporting Information, Section S3). In the case that a particle consists of highly viscous material, the reactant diffusivity became slow enough that the reacto-diffusion length was shorter than the characteristic size L of the particle. Reaction occurred prior to full mixing and a concentration gradient developed inside the volume of the particle, meaning that only a partial volume of the particle was effectively accessible to reaction (Figure 1a, left). By comparison, for a particle composed a liquid of low viscosity, the reacto-diffusion length was much larger than L, meaning that the reactant was well mixed and the entire volume of the particle was accessible to reaction (Figure 1a, right).

The reacto-diffusion lengths and the accessible reaction volume were modeled as a function of RH for two sets of parameters representing ammonia exposure in different experimental configurations (Supporting Information, Figure S2 and Table S1). The first set represented the experiments conducted in the continuous-flow mixing volume for SOM particles in aerosol form (Experiment 1). The second set represented the experiments for SOM thin films (Experiment 2). These two sets of experiments differed in gas-phase ammonia concentrations, characteristic length scales (i.e., particle size or film thickness), and exposure times. Model results and a comparison to the measurements are plotted in Figure 2c, 2d1, and 2d2. Red shading represents the range of model outputs for a Monte Carlo approach to the uncertainty of each input parameter. The observations lie within the shaded region representing model results. Although the model herein makes several simplify assumptions, the success in capturing the observations supports the hypothesis that reactant diffusivities, including both the diffusivity of small NH_3 molecules and the diffusivity of large organic molecules, can control overall rates of condensed-phase reaction rates and browning reactions. For RH < 20%, the reacto-diffusion lengths of both ammonia and the SOM molecules were shorter than the radius of typical atmospheric particles in the accumulation mode (Figure 1a, left, and Supporting Information, Figure S2). Ammonia completely reacted in the surface region of the particle. At the same time, the mass transfer of organonitrogen reaction products into the interior of the SOM and the mass-transfer replacement by fresh organic reactants from the interior were both slow. The accessible reactive volume was smaller than 10% of the total particle volume, and consequently the overall rate of reaction was limited by diffusion (Supporting Information, Section S3 and Figure S2b). By comparison, for RH > 65% the reacto-diffusion lengths of NH_3 as well as SOM molecules were modeled to increase to 10^2 nm and 10^4 nm, respectively, indicating that these reactants would be well mixed in accumulation-mode atmospheric particles and that mass transfer would not limit the overall rate of reaction.

A simulation was carried out for extension to ambient conditions. For urban environments, a gas-phase NH_3 concentration of 10 ppb is typical, and aromatic precursors are abundant.[70] Particle diameter in the simulation was varied from 30 to 1000 nm.[71] In the absence of diffusion limitations, the estimated time for reaction (i.e., browning) was modeled as 15 h (Supporting Information, Section S3 and Table S1). This case represented high RH (>80%) for which the whole particle volume was accessible to reaction (Figure S2b). For low RH (<20%), the volume accessible to rapid reaction (i.e., at the maximum rate) was <20% (Figure S2b), and the estimated time to complete browning reactions throughout the particle volume exceeded several days. Slow browning under these conditions could be entirely offset by the rapid photobleaching reactions in the atmosphere.[72] For both low and high RH, the reacto-diffusion length of the organic species was modeled as the chief regulator of the volume accessible to reaction. The reacto-diffusion length of the organic species was estimated as 1 order of magnitude greater than that of NH_3 (Figure S2a), even as the diffusivity of NH_3 was several orders of magnitude higher than that of the organic species (Figure 3). The explanation is that the concentration of NH_3 at the particle surface could not exceed that prescribed by Henry's law, and this concentration was many orders of magnitude lower than

DOI: 10.1021/acscentsci.7b00452
ACS Cent. Sci. 2018, 4, 207−215

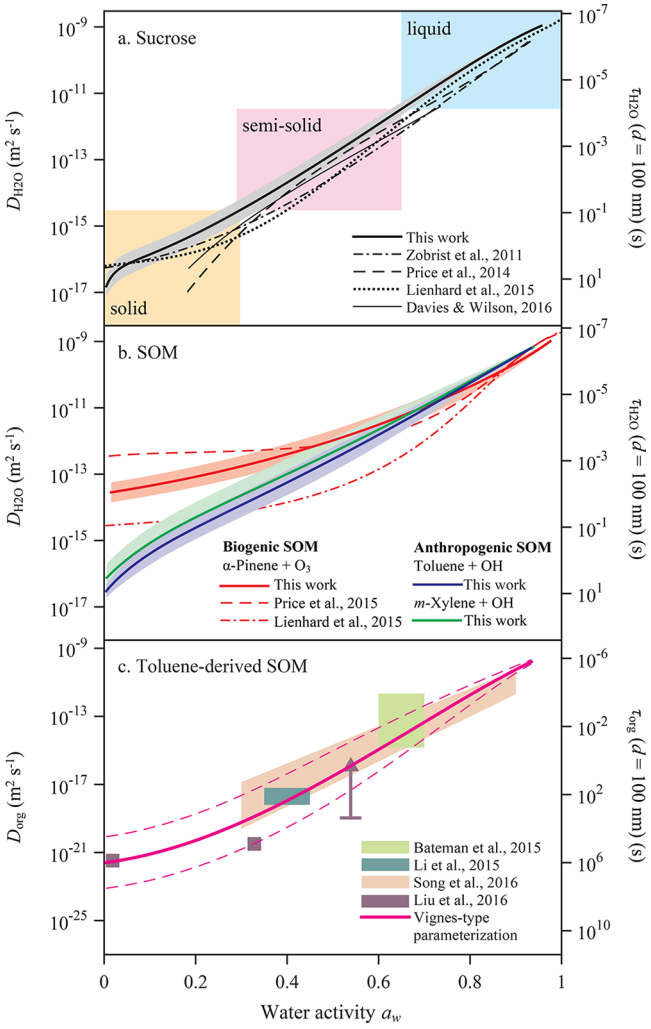

Figure 3. Diffusivity (left axis) and mixing time scale (right axis) for a 100 nm particle at 293 K. (a) Water diffusivity D_{H_2O} and mixing time scale τ_{H_2O} for the reference compound of sucrose. (b) Water diffusivity and mixing time scale for several types of secondary organic material (SOM). (c) Diffusivity D_{org} of large organic molecules and mixing time scale τ_{org} for toluene-derived SOM. Shading in panel (a) represents estimated domains of solid, semisolid, and liquid states. Shading in panel (b) represents uncertainty in the determination of $D_{H_2O}(a_w)$ (this work). The dashed pink lines in panel (c) represent the uncertainty of the Vignes parametrization, as estimated from a Monte Carlo simulation. Parameters are presented in Table S3.

that of the reactive organic species constituent to the particle (cf. Supporting Information, Section S3 and Table S1). As a result, the reaction time scale and likewise the reacto-diffusion length of the organic species was much longer than those of NH_3.

2.2. Diffusivities of Small and Large Molecules in the SOM Matrix. For the model of accessible reaction volume, estimates of the diffusivities of small and large molecules were employed. The diffusivity values D_{H_2O} of water, measured in this study and representative of a small molecule, were taken as a surrogate for those of NH_3, given the similarities between NH_3 and H_2O in molecular weight and hydrogen bonding (section 2.2.1). The diffusivity values of organic species D_{org} were estimated based on previous studies on viscosity,[40] evaporation of semivolatile compounds,[56] and rates of reactive uptake[25] (section 2.2.2).

2.2.1. Small-Molecule Diffusivities. Small-molecule diffusivity, as represented by water, was probed based on the rates of water evaporation from SOM organic films. The retrieved water diffusivity values were then tested and validated against observed rates of water condensation to SOM films. Water diffusivity values were used to represent the values of ammonia diffusivity within SOM particles. The films were grown by deposition of SOM aerosol particles on quartz crystal substrates. The aerosol particles were produced by the oxidation of volatile organic compounds (VOCs) in a flow reactor (Supporting Information, Section S1 and Figure S1).[17,73,74] Toluene photo-oxidation, *m*-xylene photo-oxidation, and α-pinene ozonolysis were studied (Table S2). The diffusivity data set for toluene-derived SOM was used in the model. The results for other types of SOM are presented herein for comparison.

Grown films were exposed to a series of humidification and drying cycles at 293.15 ± 0.1 K, and mass changes because of water uptake or release were continuously monitored by a quartz-crystal microbalance (Figure S3). Water diffusivity D_{H_2O} was retrieved from these measurements using a diffuso-kinetic model applied to the evaporation data sets during drying (cf. Supporting Information, Section S4). The D_{H_2O} values depended on water content, and a Vignes form was assumed in the model (Supporting Information, Section S4.5).[75] The Vignes form was based on diffusivities in pure water and dry material along with a nonideal mixing rule. The parameters were optimized by fitting the modeled water desorption rates to the measurements (Supporting Information, Figure S4 and Table S3). The D_{H_2O} values were further associated with water activity a_w, taken as RH/100, using the hygroscopic growth curves measured for equilibrium states (Figure S5).

As a test of the method, $D_{H_2O}(a_w)$ results obtained for sucrose in this study compared to previous studies are plotted in Figure 3a. There is good agreement. Sucrose undergoes a moisture-induced glass transition at $a_w = 0.3$ at 293 K.[50] Figure 3a shows that the corresponding D_{H_2O} value at this transition is 3×10^{-15} m^2 s^{-1}.[76] This value of D_{H_2O} serves as an approximate reference herein for the glass transition. In addition, for the measurements of the SOM films, the retrieved D_{H_2O} values obtained when drying were subsequently checked by modeling water uptake when humidifying, and there was good agreement between predictions and observations (Supporting Information, Figure S3).

The $D_{H_2O}(a_w)$ results are plotted in Figure 3b for the three types of SOM of this study. The shading represents uncertainty. Comparison to available data sets in literature are also shown. Figure 3b shows that the approximate reference value of D_{H_2O} for the glass transition occurs at $a_w = 0.2$ for toluene-derived and *m*-xylene derived SOM, implying that these aromatic-derived SOMs are highly viscous under low RH. In agreement, Song et al.[40] observed that toluene-derived SOM particles shattered when poked at 17% RH, demonstrating a brittle material.

The $D_{H_2O}(a_w)$ values of toluene-derived and *m*-xylene-derived SOMs are similar to one another (cf. Figure 3b). These results might then at least to some extent be generalizable to SOM derived from other aromatic precursors,

DOI: 10.1021/acscentsci.7b00452
ACS Cent. Sci. 2018, 4, 207−215

which are largely of anthropogenic origin. By comparison, the $D_{H_2O}(a_w)$ values for α-pinene-derived SOM, as a representative of biogenic sources, are significantly greater for $a_w < 0.65$ (Figure 3b). These differences between anthropogenic and biogenic precursors are further highlighted in recent literature.[56,58]

For $a_w > 0.65$, the $D_{H_2O}(a_w)$ values become similar among the three SOMs, and based on shifts in particle rebound the SOMs are liquid in this regime (i.e., $\eta < 10^2$ Pa s).[36] The semisolid-to-liquid transition for sucrose also occurs at $a_w = 0.65$. The in-common a_w value of 0.65 for the semisolid-to-liquid transition among these systems appears, however, to be coincidental. For instance, the transition for isoprene-derived SOM, based on rebound, occurs at $a_w = 0.40$.[36]

In Figure 3b the $D_{H_2O}(a_w)$ values reported herein are compared to the $D_{H_2O}(a_w)$ results reported by Price et al.[77] and Lienhard et al.[51] for α-pinene ozonolysis. There is agreement among all studies for $a_w > 0.8$ but significant differences for lower activities. The values reported in the literature deviate from each other by up to 2 orders of magnitude for low a_w (<0.2), and the results of the present study lie midway between the two literature results. The spread in values can arise from several factors. Price et al.[77] extracted filter samples using water, Lienhard et al.[51] extracted samples using methanol, and the SOM characterized herein was total SOM without extraction. The chemical composition and hence properties of the extracted SOM can differ from that of total SOM.[41] Another possibility is that the composition can differ among SOMs prepared differently. For instance, the O:C atomic ratio depends on conditions of production.[78] These different factors can affect the differing $D_{H_2O}(a_w)$ results among the studies. A common result among all three studies, however, is that $D_{H_2O}(a_w)$ values of biogenically α-pinene-derived SOM at the dry state ($a_w < 0.05$) are significantly higher than the corresponding values of the studied anthropogenically aromatic-derived SOMs and sucrose.

2.2.2. Large-Molecule Diffusivities. Compared to the diffusivities of small molecules, the diffusivities D_{org} of the large organic molecules can be orders of magnitude smaller. They likewise can depend on the water activity (i.e., the water content).[48] Estimated values of $D_{org}(a_w)$ for the large molecules making up toluene-derived SOM are plotted in Figure 3c. These estimates are based on several different approaches, including (1) diffusivity estimated from viscosity based on the Stokes−Einstein equation,[36,40] (2) diffusivity estimated from evaporation rates,[56] and (3) diffusivity estimated based on rates of reactive uptake.[25] The different approaches agree within an order of magnitude. The parameters of a Vignes-form fit of $D_{org}(a_w)$, optimized to the data plotted in Figure 3c, are listed in Table S3. The fit is shown in Figure 3c as the pink line, and uncertainty based on the underlying data is represented by the dashed lines. Panels (a) to (c) of Figure 3 confirm that for fixed a_w $D_{org}(a_w)$ is 10^4 to 10^6 times smaller than small-molecule diffusivity represented by $D_{H_2O}(a_w)$. The largest differences in D_{org} between small and large molecules are for the lowest a_w.

2.2.3. Mixing Times. Diffusivity can be used to estimate the characteristic mixing time τ within a particle under the assumption of rapid Henry's law equilibration between the gas phase and surface region of the particle and in the absence of a chemical reaction, as follows:[79]

$$\tau = \frac{L^2}{\pi^2 D} \quad (1)$$

where L is the geometric radius of a spherical nonporous particle and D is the diffusivity. The mixing times for 100 nm particles are given on the right axes of Figure 3a−c for the diffusivity values listed on the left axes. Atmospheric processes, such as water uptake and cloud activation, establish reference time scales, which are typically considered longer than 1 min.

The analysis represented in Figure 3b suggests that the mixing times for a small molecule represented by water throughout the volume of 100 nm particles composed of toluene-derived SOM and α-pinene-derived SOM are 10 and 0.01 s, respectively, for $a_w = 0.05$ at 293 K. Compared to the reference time scale of 1 min, small-molecule diffusion is effectively facile at 293 K even in the highly viscous material. The implication is that diffusion is kinetically impeded but not arrested on time scales relevant to atmospheric processes.[43,76] For higher a_w, mixing times are effectively instantaneous for small molecules with respect to most commonly considered atmospheric processes. To the extent that the SOM particles studied herein represent surrogates of atmospheric organic PM, the conclusion is that in the absence of in-particle chemical reactions, small molecules reach homogeneous concentrations effectively instantaneously within such particles for the temperatures and water activities relevant to most conditions of the atmospheric boundary layer.[80] For lower temperatures representative of the upper free troposphere, diffusivities can significantly decrease and mixing times can be significantly longer.[76]

The right axis of Figure 3c represents the mixing time of eq 1 for large organic molecules within 100 nm particles of toluene-derived SOM. The mixing time exceeds the characteristic time of atmospheric relevance (1 min) for $a_w \leq 0.4$. The implication is that in-particle diffusion can limit the mass transfer of organic molecules in the gas-particle partitioning processes.[56] One possible effect under atmospheric conditions is that the evolution of number-diameter distribution of the particle population can be affected.[81]

3. CONCLUSIONS

Predicting the production of brown carbon in the atmosphere and the evolution of its optical properties is challenging and remains highly uncertain. Many complex processes must be considered. The results of the present study imply that the lack of information about the species diffusivities within organic PM can be one factor, among many others, that contributes to these uncertainties. Species diffusivities can also influence other important atmospheric processes, including multiphase chemistry. Uptake and in-particle diffusion of small-molecule atmospheric photo-oxidants like OH, O_3, and NO_3 within a large-molecule environment of atmospheric PM are commonplace.[27,61,82,83] Slow species diffusivities in the organic matrix can impede these multiphase chemical reactions. In that context, the results presented herein further highlight that anthropogenic contributions to atmospheric PM appear to favor more viscous states and reduced diffusivities compared to biogenic SOM, suggesting an underestimated or overlooked pathway of human influences on atmospheric chemistry and climate.[56,58]

DOI: 10.1021/acscentsci.7b00452
ACS Cent. Sci. 2018, 4, 207−215

■ ASSOCIATED CONTENT

Supporting Information

The Supporting Information is available free of charge on the ACS Publications website at DOI: 10.1021/acscentsci.7b00452.

Experimental methods, description of the kinetic model, supplementary tables and figures (PDF)

■ AUTHOR INFORMATION

Corresponding Author

*E-mail: scot_martin@harvard.edu.

ORCID

Pengfei Liu: 0000-0001-7280-9720

Notes

The authors declare no competing financial interest.

■ ACKNOWLEDGMENTS

Mary Gilles, Suzane S. de Sá, Yuemei Han, Xue Bai, Onye Ahanotu, and Jiaxi Cui provided helpful discussion and assistance with some experiments. This research was funded by the Atmospheric System Research Program of the Office of Science of the Department of Energy (DE-SC0012792) and by the Geosciences Directorate of the National Science Foundation (AGS-1249565). P.L. was supported by a NASA Earth and Space Science Fellowship Program. The QCM experiments were performed at the Material Characterization Core of the Wyss Institute for Biologically Inspired Engineering at Harvard University.

■ REFERENCES

(1) IPCC. *Climate Change 2013: The Physical Science Basis*; Cambridge University Press: Cambridge, UK, and New York, 2013; p 1535.

(2) Dockery, D. W.; Pope, C. A.; Xu, X.; Spengler, J. D.; Ware, J. H.; Fay, M. E.; Ferris, B. G. J.; Speizer, F. E. An Association between Air Pollution and Mortality in Six U.S. Cities. *N. Engl. J. Med.* **1993**, *329* (24), 1753−1759.

(3) Shi, L.; Zanobetti, A.; Kloog, I.; Coull, B. A.; Koutrakis, P.; Melly, S. J.; Schwartz, J. D. Low-Concentration PM(2.5) and Mortality: Estimating Acute and Chronic Effects in a Population-Based Study. *Environ. Health Perspect.* **2016**, *124* (1), 46−52.

(4) Liu, Y.; Kuwata, M.; McKinney, K. A.; Martin, S. T. Uptake and release of gaseous species accompanying the reactions of isoprene photo-oxidation products with sulfate particles. *Phys. Chem. Chem. Phys.* **2016**, *18* (3), 1595−1600.

(5) Liu, Y.; Liggio, J.; Staebler, R.; Li, S. M. Reactive uptake of ammonia to secondary organic aerosols: kinetics of organonitrogen formation. *Atmos. Chem. Phys.* **2015**, *15* (23), 13569−13584.

(6) Zhang, Q.; Jimenez, J. L.; Canagaratna, M. R.; Allan, J. D.; Coe, H.; Ulbrich, I.; Alfarra, M. R.; Takami, A.; Middlebrook, A. M.; Sun, Y. L.; Dzepina, K.; Dunlea, E.; Docherty, K.; DeCarlo, P. F.; Salcedo, D.; Onasch, T.; Jayne, J. T.; Miyoshi, T.; Shimono, A.; Hatakeyama, S.; Takegawa, N.; Kondo, Y.; Schneider, J.; Drewnick, F.; Borrmann, S.; Weimer, S.; Demerjian, K.; Williams, P.; Bower, K.; Bahreini, R.; Cottrell, L.; Griffin, R. J.; Rautiainen, J.; Sun, J. Y.; Zhang, Y. M.; Worsnop, D. R. Ubiquity and dominance of oxygenated species in organic aerosols in anthropogenically-influenced Northern Hemisphere midlatitudes. *Geophys. Res. Lett.* **2007**, *34* (13), L13801.

(7) Jimenez, J. L.; Canagaratna, M. R.; Donahue, N. M.; Prevot, A. S. H.; Zhang, Q.; Kroll, J. H.; DeCarlo, P. F.; Allan, J. D.; Coe, H.; Ng, N. L.; Aiken, A. C.; Docherty, K. S.; Ulbrich, I. M.; Grieshop, A. P.; Robinson, A. L.; Duplissy, J.; Smith, J. D.; Wilson, K. R.; Lanz, V. A.; Hueglin, C.; Sun, Y. L.; Tian, J.; Laaksonen, A.; Raatikainen, T.; Rautiainen, J.; Vaattovaara, P.; Ehn, M.; Kulmala, M.; Tomlinson, J. M.; Collins, D. R.; Cubison, M. J.; Dunlea, J.; Huffman, J. A.; Onasch, T. B.; Alfarra, M. R.; Williams, P. I.; Bower, K.; Kondo, Y.; Schneider, J.; Drewnick, F.; Borrmann, S.; Weimer, S.; Demerjian, K.; Salcedo, D.; Cottrell, L.; Griffin, R.; Takami, A.; Miyoshi, T.; Hatakeyama, S.; Shimono, A.; Sun, J. Y.; Zhang, Y. M.; Dzepina, K.; Kimmel, J. R.; Sueper, D.; Jayne, J. T.; Herndon, S. C.; Trimborn, A. M.; Williams, L. R.; Wood, E. C.; Middlebrook, A. M.; Kolb, C. E.; Baltensperger, U.; Worsnop, D. R. Evolution of Organic Aerosols in the Atmosphere. *Science* **2009**, *326* (5959), 1525−1529.

(8) Andreae, M. O.; Gelencsér, A. Black carbon or brown carbon? The nature of light-absorbing carbonaceous aerosols. *Atmos. Chem. Phys.* **2006**, *6* (10), 3131−3148.

(9) Moise, T.; Flores, J. M.; Rudich, Y. Optical Properties of Secondary Organic Aerosols and Their Changes by Chemical Processes. *Chem. Rev.* **2015**, *115* (10), 4400−4439.

(10) Sun, H.; Biedermann, L.; Bond, T. C. Color of brown carbon: A model for ultraviolet and visible light absorption by organic carbon aerosol. *Geophys. Res. Lett.* **2007**, *34* (17), L17813.

(11) Liu, P.; Zhang, Y.; Martin, S. T. Complex refractive indices of thin films of secondary organic materials by spectroscopic ellipsometry from 220 to 1200 nm. *Environ. Sci. Technol.* **2013**, *47* (23), 13594−13601.

(12) Lin, G.; Penner, J. E.; Flanner, M. G.; Sillman, S.; Xu, L.; Zhou, C. Radiative forcing of organic aerosol in the atmosphere and on snow: Effects of SOA and brown carbon. *J. Geophys. Res.: Atmos.* **2014**, *119* (12), 7453.

(13) Liu, J.; Scheuer, E.; Dibb, J.; Ziemba, L. D.; Thornhill, K. L.; Anderson, B. E.; Wisthaler, A.; Mikoviny, T.; Devi, J. J.; Bergin, M.; Weber, R. J. Brown carbon in the continental troposphere. *Geophys. Res. Lett.* **2014**, *41* (6), 2191.

(14) Bond, T. C.; Bergstrom, R. W. Light Absorption by Carbonaceous Particles: An Investigative Review. *Aerosol Sci. Technol.* **2006**, *40* (1), 27−67.

(15) Lack, D. A.; Langridge, J. M.; Bahreini, R.; Cappa, C. D.; Middlebrook, A. M.; Schwarz, J. P. Brown carbon and internal mixing in biomass burning particles. *Proc. Natl. Acad. Sci. U. S. A.* **2012**, *109* (37), 14802−14807.

(16) Updyke, K. M.; Nguyen, T. B.; Nizkorodov, S. A. Formation of brown carbon via reactions of ammonia with secondary organic aerosols from biogenic and anthropogenic precursors. *Atmos. Environ.* **2012**, *63* (0), 22−31.

(17) Liu, P. F.; Abdelmalki, N.; Hung, H. M.; Wang, Y.; Brune, W. H.; Martin, S. T. Ultraviolet and visible complex refractive indices of secondary organic material produced by photooxidation of the aromatic compounds toluene and m-xylene. *Atmos. Chem. Phys.* **2015**, *15* (3), 1435−1446.

(18) Lin, Y.-H.; Budisulistiorini, S. H.; Chu, K.; Siejack, R. A.; Zhang, H.; Riva, M.; Zhang, Z.; Gold, A.; Kautzman, K. E.; Surratt, J. D. Light-absorbing oligomer formation in secondary organic aerosol from reactive uptake of isoprene epoxydiols. *Environ. Sci. Technol.* **2014**, *48* (20), 12012−12021.

(19) Zarzana, K. J.; De Haan, D. O.; Freedman, M. A.; Hasenkopf, C. A.; Tolbert, M. A. Optical Properties of the Products of α-Dicarbonyl and Amine Reactions in Simulated Cloud Droplets. *Environ. Sci. Technol.* **2012**, *46* (9), 4845−4851.

(20) Lin, P.; Laskin, J.; Nizkorodov, S. A.; Laskin, A. Revealing Brown Carbon Chromophores Produced in Reactions of Methylglyoxal with Ammonium Sulfate. *Environ. Sci. Technol.* **2015**, *49* (24), 14257−14266.

(21) Nguyen, T. B.; Lee, P. B.; Updyke, K. M.; Bones, D. L.; Laskin, J.; Laskin, A.; Nizkorodov, S. A. Formation of nitrogen- and sulfur-containing light-absorbing compounds accelerated by evaporation of water from secondary organic aerosols. *J. Geophys. Res.: Atmos.* **2012**, *117* (D1), D01207.

(22) Forrister, H.; Liu, J.; Scheuer, E.; Dibb, J.; Ziemba, L.; Thornhill, K. L.; Anderson, B.; Diskin, G.; Perring, A. E.; Schwarz, J. P.; Campuzano-Jost, P.; Day, D. A.; Palm, B. B.; Jimenez, J. L.; Nenes, A.; Weber, R. J. Evolution of brown carbon in wildfire plumes. *Geophys. Res. Lett.* **2015**, *42* (11), 4623−4630.

(23) Nguyen, T. B.; Laskin, A.; Laskin, J.; Nizkorodov, S. A. Brown carbon formation from ketoaldehydes of biogenic monoterpenes. *Faraday Discuss.* **2013**, *165* (0), 473−494.
(24) Romonosky, D. E.; Ali, N. N.; Saiduddin, M. N.; Wu, M.; Lee, H. J.; Aiona, P. K.; Nizkorodov, S. A. Effective absorption cross sections and photolysis rates of anthropogenic and biogenic secondary organic aerosols. *Atmos. Environ.* **2016**, *130*, 172−179.
(25) Li, Y. J.; Liu, P.; Gong, Z.; Wang, Y.; Bateman, A. P.; Bergoend, C.; Bertram, A. K.; Martin, S. T. Chemical reactivity and liquid/non-liquid states of secondary organic material. *Environ. Sci. Technol.* **2015**, *49* (22), 13264−13274.
(26) Kuwata, M.; Martin, S. T. Phase of atmospheric secondary organic material affects its reactivity. *Proc. Natl. Acad. Sci. U. S. A.* **2012**, *109* (43), 17354−17359.
(27) Shiraiwa, M.; Ammann, M.; Koop, T.; Pöschl, U. Gas uptake and chemical aging of semisolid organic aerosol particles. *Proc. Natl. Acad. Sci. U. S. A.* **2011**, *108* (27), 11003−11008.
(28) Lignell, H.; Hinks, M. L.; Nizkorodov, S. A. Exploring matrix effects on photochemistry of organic aerosols. *Proc. Natl. Acad. Sci. U. S. A.* **2014**, *111* (38), 13780−13785.
(29) Hinks, M. L.; Brady, M. V.; Lignell, H.; Song, M.; Grayson, J. W.; Bertram, A. K.; Lin, P.; Laskin, A.; Laskin, J.; Nizkorodov, S. A. Effect of viscosity on photodegradation rates in complex secondary organic aerosol materials. *Phys. Chem. Chem. Phys.* **2016**, *18* (13), 8785−8793.
(30) Donahue, N. M.; Robinson, A. L.; Stanier, C. O.; Pandis, S. N. Coupled partitioning, dilution, and chemical aging of semivolatile organics. *Environ. Sci. Technol.* **2006**, *40* (8), 2635−2643.
(31) Virtanen, A.; Joutsensaari, J.; Koop, T.; Kannosto, J.; Yli-Pirila, P.; Leskinen, J.; Makela, J. M.; Holopainen, J. K.; Poschl, U.; Kulmala, M.; Worsnop, D. R.; Laaksonen, A. An amorphous solid state of biogenic secondary organic aerosol particles. *Nature* **2010**, *467* (7317), 824−827.
(32) Vaden, T. D.; Imre, D.; Beránek, J.; Shrivastava, M.; Zelenyuk, A. Evaporation kinetics and phase of laboratory and ambient secondary organic aerosol. *Proc. Natl. Acad. Sci. U. S. A.* **2011**, *108* (6), 2190−2195.
(33) Kidd, C.; Perraud, V.; Wingen, L. M.; Finlayson-Pitts, B. J. Integrating phase and composition of secondary organic aerosol from the ozonolysis of α-pinene. *Proc. Natl. Acad. Sci. U. S. A.* **2014**, *111* (21), 7552−7557.
(34) Mikhailov, E.; Vlasenko, S.; Martin, S. T.; Koop, T.; Pöschl, U. Amorphous and crystalline aerosol particles interacting with water vapor: conceptual framework and experimental evidence for restructuring, phase transitions and kinetic limitations. *Atmos. Chem. Phys.* **2009**, *9* (24), 9491−9522.
(35) Saukko, E.; Lambe, A. T.; Massoli, P.; Koop, T.; Wright, J. P.; Croasdale, D. R.; Pedernera, D. A.; Onasch, T. B.; Laaksonen, A.; Davidovits, P.; Worsnop, D. R.; Virtanen, A. Humidity-dependent phase state of SOA particles from biogenic and anthropogenic precursors. *Atmos. Chem. Phys.* **2012**, *12* (16), 7517−7529.
(36) Bateman, A. P.; Bertram, A. K.; Martin, S. T. Hygroscopic influence on the semisolid-to-liquid transition of secondary organic materials. *J. Phys. Chem. A* **2015**, *119* (19), 4386−4395.
(37) Renbaum-Wolff, L.; Grayson, J. W.; Bateman, A. P.; Kuwata, M.; Sellier, M.; Murray, B. J.; Shilling, J. E.; Martin, S. T.; Bertram, A. K. Viscosity of α-pinene secondary organic material and implications for particle growth and reactivity. *Proc. Natl. Acad. Sci. U. S. A.* **2013**, *110* (20), 8014−8019.
(38) Zhang, Y.; Sanchez, M. S.; Douet, C.; Wang, Y.; Bateman, A. P.; Gong, Z.; Kuwata, M.; Renbaum-Wolff, L.; Sato, B. B.; Liu, P. F.; Bertram, A. K.; Geiger, F. M.; Martin, S. T. Changing shapes and implied viscosities of suspended submicron particles. *Atmos. Chem. Phys.* **2015**, *15* (14), 7819−7829.
(39) Song, M.; Liu, P. F.; Hanna, S. J.; Li, Y. J.; Martin, S. T.; Bertram, A. K. Relative humidity-dependent viscosities of isoprene-derived secondary organic material and atmospheric implications for isoprene-dominant forests. *Atmos. Chem. Phys.* **2015**, *15* (9), 5145−5159.
(40) Song, M.; Liu, P. F.; Hanna, S. J.; Zaveri, R. A.; Potter, K.; You, Y.; Martin, S. T.; Bertram, A. K. Relative humidity-dependent viscosity of secondary organic material from toluene photo-oxidation and possible implications for organic particulate matter over megacities. *Atmos. Chem. Phys.* **2016**, *16* (14), 8817−8830.
(41) Grayson, J. W.; Zhang, Y.; Mutzel, A.; Renbaum-Wolff, L.; Böge, O.; Kamal, S.; Herrmann, H.; Martin, S. T.; Bertram, A. K. Effect of varying experimental conditions on the viscosity of α-pinene derived secondary organic material. *Atmos. Chem. Phys.* **2016**, *16* (10), 6027−6040.
(42) Power, R. M.; Simpson, S. H.; Reid, J. P.; Hudson, A. J. The transition from liquid to solid-like behaviour in ultrahigh viscosity aerosol particles. *Chem. Sci.* **2013**, *4* (6), 2597−2604.
(43) Price, H. C.; Murray, B. J.; Mattsson, J.; O'Sullivan, D.; Wilson, T. W.; Baustian, K. J.; Benning, L. G. Quantifying water diffusion in high-viscosity and glassy aqueous solutions using a Raman isotope tracer method. *Atmos. Chem. Phys.* **2014**, *14* (8), 3817−3830.
(44) Champion, D.; Hervet, H.; Blond, G.; Le Meste, M.; Simatos, D. Translational diffusion in sucrose solutions in the vicinity of their glass transition temperature. *J. Phys. Chem. B* **1997**, *101* (50), 10674−10679.
(45) Price, H. C.; Mattsson, J.; Murray, B. J. Sucrose diffusion in aqueous solution. *Phys. Chem. Chem. Phys.* **2016**, *18* (28), 19207−19216.
(46) Chenyakin, Y.; Ullmann, D. A.; Evoy, E.; Renbaum-Wolff, L.; Kamal, S.; Bertram, A. K. Diffusion coefficients of organic molecules in sucrose−water solutions and comparison with Stokes−Einstein predictions. *Atmos. Chem. Phys.* **2017**, *17* (3), 2423−2435.
(47) LeBoeuf, E. J.; Weber, W. J. Macromolecular Characteristics of Natural Organic Matter. 1. Insights from Glass Transition and Enthalpic Relaxation Behavior. *Environ. Sci. Technol.* **2000**, *34* (17), 3623−3631.
(48) Koop, T.; Bookhold, J.; Shiraiwa, M.; Poschl, U. Glass transition and phase state of organic compounds: dependency on molecular properties and implications for secondary organic aerosols in the atmosphere. *Phys. Chem. Chem. Phys.* **2011**, *13* (43), 19238−19255.
(49) Dette, H. P.; Qi, M.; Schröder, D. C.; Godt, A.; Koop, T. Glass-Forming Properties of 3-Methylbutane-1,2,3-tricarboxylic Acid and Its Mixtures with Water and Pinonic Acid. *J. Phys. Chem. A* **2014**, *118* (34), 7024−7033.
(50) Zobrist, B.; Marcolli, C.; Pedernera, D. A.; Koop, T. Do atmospheric aerosols form glasses? *Atmos. Chem. Phys.* **2008**, *8* (17), 5221−5244.
(51) Lienhard, D. M.; Huisman, A. J.; Krieger, U. K.; Rudich, Y.; Marcolli, C.; Luo, B. P.; Bones, D. L.; Reid, J. P.; Lambe, A. T.; Canagaratna, M. R.; Davidovits, P.; Onasch, T. B.; Worsnop, D. R.; Steimer, S. S.; Koop, T.; Peter, T. Viscous organic aerosol particles in the upper troposphere: diffusivity-controlled water uptake and ice nucleation? *Atmos. Chem. Phys.* **2015**, *15* (23), 13599−13613.
(52) Murray, B. J. Inhibition of ice crystallisation in highly viscous aqueous organic acid droplets. *Atmos. Chem. Phys.* **2008**, *8* (17), 5423−5433.
(53) Murray, B. J.; Wilson, T. W.; Dobbie, S.; Cui, Z.; Al-Jumur, S. M. R. K.; Mohler, O.; Schnaiter, M.; Wagner, R.; Benz, S.; Niemand, M.; Saathoff, H.; Ebert, V.; Wagner, S.; Karcher, B. Heterogeneous nucleation of ice particles on glassy aerosols under cirrus conditions. *Nat. Geosci.* **2010**, *3* (4), 233−237.
(54) Wang, B.; Lambe, A. T.; Massoli, P.; Onasch, T. B.; Davidovits, P.; Worsnop, D. R.; Knopf, D. A. The deposition ice nucleation and immersion freezing potential of amorphous secondary organic aerosol: Pathways for ice and mixed-phase cloud formation. *J. Geophys. Res.: Atmos.* **2012**, *117* (D16), D16209.
(55) Shiraiwa, M.; Li, Y.; Tsimpidi, A. P.; Karydis, V. A.; Berkemeier, T.; Pandis, S. N.; Lelieveld, J.; Koop, T.; Pöschl, U. Global distribution of particle phase state in atmospheric secondary organic aerosols. *Nat. Commun.* **2017**, *8*, 15002.

DOI: 10.1021/acscentsci.7b00452
ACS Cent. Sci. 2018, 4, 207−215

(56) Liu, P.; Li, Y. J.; Wang, Y.; Gilles, M. K.; Zaveri, R. A.; Bertram, A. K.; Martin, S. T. Lability of secondary organic particulate matter. *Proc. Natl. Acad. Sci. U. S. A.* **2016**, *113* (45), 12643−12648.
(57) Bateman, A. P.; Gong, Z.; Liu, P.; Sato, B.; Cirino, G.; Zhang, Y.; Artaxo, P.; Bertram, A. K.; Manzi, A. O.; Rizzo, L. V.; Souza, R. A. F.; Zaveri, R. A.; Martin, S. T. Sub-micrometre particulate matter is primarily in liquid form over Amazon rainforest. *Nat. Geosci.* **2016**, *9* (1), 34−37.
(58) Ye, Q.; Robinson, E. S.; Ding, X.; Ye, P.; Sullivan, R. C.; Donahue, N. M. Mixing of secondary organic aerosols versus relative humidity. *Proc. Natl. Acad. Sci. U. S. A.* **2016**, *113* (45), 12649−12654.
(59) Shiraiwa, M.; Pfrang, C.; Pöschl, U. Kinetic multi-layer model of aerosol surface and bulk chemistry (KM-SUB): the influence of interfacial transport and bulk diffusion on the oxidation of oleic acid by ozone. *Atmos. Chem. Phys.* **2010**, *10* (8), 3673−3691.
(60) Zhou, S.; Shiraiwa, M.; McWhinney, R. D.; Poschl, U.; Abbatt, J. P. D. Kinetic limitations in gas-particle reactions arising from slow diffusion in secondary organic aerosol. *Faraday Discuss.* **2013**, *165* (0), 391−406.
(61) Davies, J. F.; Wilson, K. R. Nanoscale interfacial gradients formed by the reactive uptake of OH radicals onto viscous aerosol surfaces. *Chem. Sci.* **2015**, *6* (12), 7020−7027.
(62) Berkemeier, T.; Steimer, S. S.; Krieger, U. K.; Peter, T.; Poschl, U.; Ammann, M.; Shiraiwa, M. Ozone uptake on glassy, semi-solid and liquid organic matter and the role of reactive oxygen intermediates in atmospheric aerosol chemistry. *Phys. Chem. Chem. Phys.* **2016**, *18* (18), 12662−12674.
(63) Worsnop, D. R.; Morris, J. W.; Shi, Q.; Davidovits, P.; Kolb, C. E. A chemical kinetic model for reactive transformations of aerosol particles. *Geophys. Res. Lett.* **2002**, *29* (20), 57-1−57-14.
(64) Ng, N. L.; Kroll, J. H.; Chan, A. W. H.; Chhabra, P. S.; Flagan, R. C.; Seinfeld, J. H. Secondary organic aerosol formation from m-xylene, toluene, and benzene. *Atmos. Chem. Phys.* **2007**, *7* (14), 3909−3922.
(65) Lin, P.; Liu, J.; Shilling, J. E.; Kathmann, S. M.; Laskin, J.; Laskin, A. Molecular characterization of brown carbon (BrC) chromophores in secondary organic aerosol generated from photo-oxidation of toluene. *Phys. Chem. Chem. Phys.* **2015**, *17* (36), 23312−23325.
(66) Nakayama, T.; Sato, K.; Matsumi, Y.; Imamura, T.; Yamazaki, A.; Uchiyama, A. Wavelength and NOx dependent complex refractive index of SOAs generated from the photooxidation of toluene. *Atmos. Chem. Phys.* **2013**, *13* (2), 531−545.
(67) Laskin, J.; Laskin, A.; Roach, P. J.; Slysz, G. W.; Anderson, G. A.; Nizkorodov, S. A.; Bones, D. L.; Nguyen, L. Q. High-Resolution Desorption Electrospray Ionization Mass Spectrometry for Chemical Characterization of Organic Aerosols. *Anal. Chem.* **2010**, *82* (5), 2048−2058.
(68) Na, K.; Song, C.; Switzer, C.; Cocker, D. R. Effect of Ammonia on Secondary Organic Aerosol Formation from α-Pinene Ozonolysis in Dry and Humid Conditions. *Environ. Sci. Technol.* **2007**, *41* (17), 6096−6102.
(69) Cappa, C. D.; Onasch, T. B.; Massoli, P.; Worsnop, D. R.; Bates, T. S.; Cross, E. S.; Davidovits, P.; Hakala, J.; Hayden, K. L.; Jobson, B. T.; Kolesar, K. R.; Lack, D. A.; Lerner, B. M.; Li, S.-M.; Mellon, D.; Nuaaman, I.; Olfert, J. S.; Petäjä, T.; Quinn, P. K.; Song, C.; Subramanian, R.; Williams, E. J.; Zaveri, R. A. Radiative Absorption Enhancements Due to the Mixing State of Atmospheric Black Carbon. *Science* **2012**, *337* (6098), 1078−1081.
(70) Wang, S.; Nan, J.; Shi, C.; Fu, Q.; Gao, S.; Wang, D.; Cui, H.; Saiz-Lopez, A.; Zhou, B. Atmospheric ammonia and its impacts on regional air quality over the megacity of Shanghai, China. *Sci. Rep.* **2015**, *5*, 15842.
(71) Wu, Z.; Hu, M.; Lin, P.; Liu, S.; Wehner, B.; Wiedensohler, A. Particle number size distribution in the urban atmosphere of Beijing, China. *Atmos. Environ.* **2008**, *42* (34), 7967−7980.
(72) Laskin, A.; Laskin, J.; Nizkorodov, S. A. Chemistry of Atmospheric Brown Carbon. *Chem. Rev.* **2015**, *115* (10), 4335−4382.
(73) Kang, E.; Root, M. J.; Toohey, D. W.; Brune, W. H. Introducing the concept of Potential Aerosol Mass (PAM). *Atmos. Chem. Phys.* **2007**, *7* (22), 5727−5744.
(74) Lambe, A. T.; Ahern, A. T.; Williams, L. R.; Slowik, J. G.; Wong, J. P. S.; Abbatt, J. P. D.; Brune, W. H.; Ng, N. L.; Wright, J. P.; Croasdale, D. R.; Worsnop, D. R.; Davidovits, P.; Onasch, T. B. Characterization of aerosol photooxidation flow reactors: heterogeneous oxidation, secondary organic aerosol formation and cloud condensation nuclei activity measurements. *Atmos. Meas. Tech.* **2011**, *4* (3), 445−461.
(75) Vignes, A. Diffusion in Binary Solutions. Variation of Diffusion Coefficient with Composition. *Ind. Eng. Chem. Fundam.* **1966**, *5* (2), 189−199.
(76) Zobrist, B.; Soonsin, V.; Luo, B. P.; Krieger, U. K.; Marcolli, C.; Peter, T.; Koop, T. Ultra-slow water diffusion in aqueous sucrose glasses. *Phys. Chem. Chem. Phys.* **2011**, *13* (8), 3514−3526.
(77) Price, H. C.; Mattsson, J.; Zhang, Y.; Bertram, A. K.; Davies, J. F.; Grayson, J. W.; Martin, S. T.; O'Sullivan, D.; Reid, J. P.; Rickards, A. M. J.; Murray, B. J. Water diffusion in atmospherically relevant alpha-pinene secondary organic material. *Chem. Sci.* **2015**, *6* (8), 4876−4883.
(78) Shilling, J. E.; Chen, Q.; King, S. M.; Rosenoern, T.; Kroll, J. H.; Worsnop, D. R.; DeCarlo, P. F.; Aiken, A. C.; Sueper, D.; Jimenez, J. L.; Martin, S. T. Loading-dependent elemental composition of α-pinene SOA particles. *Atmos. Chem. Phys.* **2009**, *9* (3), 771−782.
(79) Seinfeld, J. H.; Pandis, S. N. *Atmospheric Chemistry and Physics: From Air Pollution to Climate Change*; John Wiley & Sons: New York, 2006.
(80) Maclean, A. M.; Butenhoff, C. L.; Grayson, J. W.; Barsanti, K.; Jimenez, J. L.; Bertram, A. K. Mixing times of organic molecules within secondary organic aerosol particles: a global planetary boundary layer perspective. *Atmos. Chem. Phys.* **2017**, *17* (21), 13037−13048.
(81) Zaveri, R. A.; Easter, R. C.; Shilling, J. E.; Seinfeld, J. H. Modeling kinetic partitioning of secondary organic aerosol and size distribution dynamics: representing effects of volatility, phase state, and particle-phase reaction. *Atmos. Chem. Phys.* **2014**, *14* (10), 5153−5181.
(82) McNeill, V. F.; Yatavelli, R. L. N.; Thornton, J. A.; Stipe, C. B.; Landgrebe, O. Heterogeneous OH oxidation of palmitic acid in single component and internally mixed aerosol particles: vaporization and the role of particle phase. *Atmos. Chem. Phys.* **2008**, *8* (17), 5465−5476.
(83) Katrib, Y.; Biskos, G.; Buseck, P. R.; Davidovits, P.; Jayne, J. T.; Mochida, M.; Wise, M. E.; Worsnop, D. R.; Martin, S. T. Ozonolysis of Mixed Oleic-Acid/Stearic-Acid Particles: Reaction Kinetics and Chemical Morphology. *J. Phys. Chem. A* **2005**, *109* (48), 10910−10919.

DOI: 10.1021/acscentsci.7b00452
ACS Cent. Sci. 2018, 4, 207−215